Electronic structure and total-energy migration barriers of silicon self-interstitials

Y. Bar-Yam and J. D. Joannopoulos
Department of Physics, Massachusetts Institute of Technology, Cambridge, Massachusetts 02139
(Received 20 March 1984)

Pseudopotential density-functional calculations have been performed on silicon self-interstitial supercell model geometries to yield extensive information on electronic states. We present band structures, charge densities, and densities of states to identify and characterize electronic states associated with silicon self-interstitials in the geometries studied. Total energies obtained yield migration barriers for both $Si^{(0)}$ and $Si^{(2+)}$ interstitials. We also present the results of preliminary total-energy relaxation studies and show their effects on electronic states and total-energy calculations, demonstrating the importance of relaxation in determining migration barriers. Electron-assisted migration is shown to occur, thus solving the mystery of the disappearing self-interstitial and providing an initial understanding of migration in low-temperature irradiated silicon.

I. INTRODUCTION

Understanding point defects in semiconductors is one of the most exciting challenges currently facing condensed-matter theory. Even in silicon, the most studied semiconductor both experimentally and theoretically, our understanding of the electronic states and formation and migration energetics of point defects is still primitive.

Total-energy pseudopotential density-functional calculations are currently the most powerful tool for the calculation of ground-state properties of crystals.[1] Recently, the scope of calculations has been extended to the study of surfaces,[2] interfaces,[3] and defects.[4] Here, we report a study of defect migration.[5]

Silicon self-interstitial migration has been an interesting subject for two decades. In 1964 Watkins *et al.*[6] began a study of low-temperature irradiated silicon which provided considerable information and several interesting puzzles about defects and their migration. Among these puzzles was the lack of detection of self-interstitials. Self-interstitials were not detected even at 4.2 K when vacancies were detected in large numbers. Since interstitials must be created, the lack of detection presented a mystery. An important clue was the detection of interstitial aluminum impurity atoms which are normally substitutional. Thus, it was suggested that interstitial silicon could migrate at high speeds even at such low temperatures, and upon encountering substitutional Al the silicon interstitial would kick the Al out of the lattice into the interstices and replace it.

The important question then became how could the migration of self-interstitials proceed rapidly at low temperatures? One possibility is that the migration barrier is very low so that even at 4.2 K migration could proceed thermally. However, such a low barrier is inconsistent with high-temperature diffusion results, which indicate a significant energy barrier.[7]

Several suggestions were made to resolve this difficulty. One of these proposed that electron-assisted transport might enable transport even if the barriers were high. The argument proceeds by recognizing that in low-temperature irradiated samples there is a lot of energy in the form of electrons in excited states. This energy can lead to migration if there are different possible charge states of a defect which have different migration barriers or minimum-energy positions. Electron-assisted transport was proposed and various possible mechanisms were detailed by Bourgoin and Corbett.[8] Electron-assisted transport is now considered to be a very common occurrence for many defects, including the silicon vacancy and aluminum interstitials in silicon.[9]

In 1971 simple electronic energy extended Hückel theory (EHT) calculations with only nearest-neighbor interactions were performed by Watkins *et al.*[10] on the silicon self-interstitial. These calculations indicated a very large energy difference (10 eV) along the previously generally assumed path of migration, which is the path through the low-electron-density regions of the crystal. Using their results they proposed a path through the bonds as a candidate for electron-assisted migrations.

These theoretical results were challenged recently by Pantelides *et al.*,[11] who demonstrated via a Green's-function pseudopotential calculation of the tetrahedral density of states that the EHT calculations were unreliable. He further argued on the basis of effective-medium theory[12] that the low-electron-density path is a more likely low-barrier path than the path through the bonds.

In a recent paper Baraff and Schlüter[13] presented Green's-function transition-state calculations for both the tetrahedral and hexagonal sites. On the basis of their calculations they were able to argue for a barrier lowering of $Si^{(2+)} \rightarrow Si^{(0)}$ of 2.2 eV. This suggested that electron-assisted migration might occur along the low-electron-density path.

In this paper we describe the first *ab initio* total-energy migration calculations. We performed calculations for both $Si^{(0)}$ and $Si^{(2+)}$ migration through the low-electron-density path. In a later publication,[14] total-energy calculations which demonstrate that this path is one of several migration paths will be described in detail.

In Sec. II we describe the calculations, methodology, and geometries. Results are presented in Secs. III and IV.

Section III contains electronic state results: band structures, densities of states, and eigenstate charge densities for unrelaxed and relaxed configurations. Total-energy migration-barrier and relaxation calculations are presented in Sec. IV. Conclusions are given in Sec. V.

II. CALCULATIONAL METHOD AND SUPERCELL GEOMETRY

In order to study the silicon self-interstitial we used two supercell geometries containing eight and sixteen crystal atoms, respectively. The superlattice in the first geometry is simple cubic and is displayed in Fig. 1; the superlattice in the second geometry is face-centered cubic (not shown). The interstitial-interstitial nearest-neighbor distances are 5.4 and 7.6 Å, respectively. All calculations were performed in both geometries, which enabled us to test the effects of the supercell model geometry on results. The interstitial was studied along the low-electron-density path which passes through the tetrahedral and hexagonal sites as shown in Fig. 1. To assist the reader in visualizing the path we show in advance (Fig. 2) the total valence charge density in the (110) plane obtained from our calculations for pure silicon and after placing the interstitial at the tetrahedral and hexagonal sites.

Electronic energies and wave functions were obtained from momentum-space diagonalization of the Hamiltonian. A plane-wave basis corresponding to an energy cutoff of 6 Ry ($\sim$550 plane waves in geometry II) was treated exactly and an additional set up to 11 Ry ($\sim$1350 total plane waves in geometry II) was included in perturbation theory.

The silicon pseudopotential used was norm conserving[15] with S,P,D nonlocal components and the core cutoff radii of Bachelet *et al.*[16] Perdew-Zunger Ceperley-Alder[17] (PZCA) correlation was used.[18]

Total energies along the migration path were obtained using the self-consistent momentum-space formalism of Ihm *et al.*[19] Special $\vec{k}$ points[20] were used for total-energy integrations. Convergence was checked in the number of $\vec{k}$ points. Equivalent sets were used for tetrahedral and hexagonal sites and for comparison between geometries I and II. Specifically, for geometry I, four $\vec{k}$ points were used at the tetrahedral site, corresponding, after symmetry breaking, to ten $\vec{k}$ points at the hexagonal site. After Brillouin-zone folding, these corresponded to two and five $\vec{k}$ points, respectively, in geometry II.

For $Si^{(2+)}$ calculations an inert (noncorrelating) uniform charge background was used to neutralize the system. This affects only the $G=0$ term of the potential (eliminating the divergence). This approximation can be directly tested, along with others, by increasing the size of the supercell. For the results reported here, which are energy differences corresponding to barrier heights and relaxation energies, this approximation was found to be extremely good.

Changes in migration barriers and relaxation energies for $Si^{(2+)}$ from geometry I to II were found to be less than 0.2 eV. This includes all errors due to the finite supercell size. The largest error (close to 0.2 eV) was for hexagonal-site relaxation where, in geometry I, nearest neighbors have neighbors which also relax due to the sys-

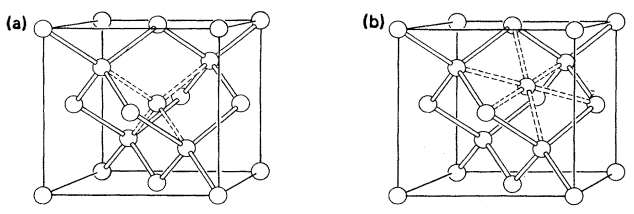

FIG. 1. Supercell geometry I with eight host atoms and an interstitial near the center. (a) Tetrahedral site. (b) Hexagonal site.

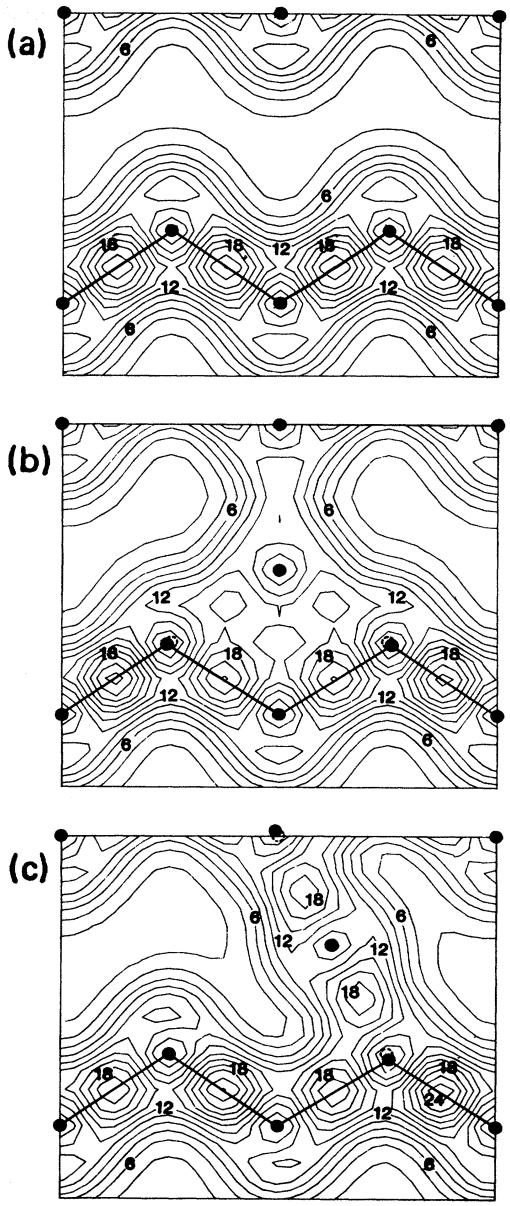

FIG. 2. Total valence charge densities (in units of electrons per bulk primitive cell) in the (110) plane for (a) pure silicon, (b) Si self-interstitial at tetrahedral site, and (c) Si self-interstitial at hexagonal site. Dashed circles in (b) and (c) represent unrelaxed atomic positions.

tem periodicity. All other errors were 0.1 eV or less.

For $Si^{(0)}$ calculations it was necessary to make a correction to the energy of the highest occupied band, which is described in the Appendix. The error due to this correction process is estimated to be less than 0.3 eV.

III. ELECTRONIC STATE RESULTS

The use of supercell geometries makes it possible to present electronic state energy eigenvalues as band structures. In comparison to the pure crystal, the Brillouin zone of the superlattice is folded smaller, in reciprocal correspondence to the enlargement of the real-space unit cell.

First, we will present results for the hypothetical case of a silicon self-interstitial in an unrelaxed host. Later, we will allow breathing-mode relaxation of nearest neighbors and investigate the effects of relaxation on the electronic structure.

A. Unrelaxed host: Geometry I

Unrelaxed crystal band structures for geometry I (Γ—L) are shown in Fig. 3. Figures 3(a) and 3(c) are for the tetrahedral and hexagonal sites, respectively. For comparison, we show the pure-silicon band structure in Fig. 3(b). Concentrating for the moment on the pure-silicon band structure, we note that in the ordinary (two-atom) unit cell of silicon, the Γ—L band structure would show only the curves shown as solid lines in Fig. 3(b). Because of the enlarged real-space unit cell of geometry I (with eight atoms per unit cell), the Brillouin zone is folded in and the segment X—$(\frac{1}{2},\frac{1}{2},\frac{3}{2})$ overlaps Γ—L. These are triply degenerate lines and they are indicated by dashed lines in Fig. 3(b).

Placing the self-interstitial in the crystal shifts bands and breaks degeneracies. We see from Figs. 3(a) and 3(c) that although the band structure is extensively modified it is still possible to associate bands with unperturbed bands in Fig. 3(b). Thus, we also use solid and dashed lines in these figures to aid in the comparison with Fig. 3(b). Note that the triply degenerate states are split into doubly and singly degenerate states. In addition to the shifting and splitting of valence-band levels, there appears in the valence band one additional level which cannot be identified with those of pure silicon (but corresponds to a conduction-band state in pure silicon), which has been indicated by a dotted line. At the hexagonal site there is an additional state which is seen to span the gap in this geometry, which is also indicated by a dotted line. These states and resonances should be clearly identified with the interstitial. Other states which have been shifted significantly will also have significant amplitude on the interstitial and will also be identified with changes in the density of states. Before describing, these states in detail, we display the band structures of geometry II.

B. Unrelaxed host: Geometry II

Unrelaxed crystal band structures for geometry II are shown in Fig. 4. Doubling the unit cell from geometry I to geometry II causes halving of the Brillouin zone. In the direction Γ—L the effect of this halving is simply to fold over the L point onto the Γ point. This unit cell corresponds exactly to an eight fold volume change over the ordinary silicon unit cell by doubling the length of primitive lattice vectors (halving the reciprocal-lattice vectors). For additional guidance in interpreting the band structures we also display rough densities of states for the tetrahedral and hexagonal sites. These are obtained by using two (five) special $\vec{k}$ points at the tetrahedral (hexagonal) site which correspond to ten $\vec{k}$ points in the ordinary unit cell of silicon. More $\vec{k}$ points would be needed for good accuracy in the density of states. However, the present number is adequate when used along with charge densities for the purpose of identifying defectlike states. (We note that the density of states for the tetrahedral site is in reasonably good agreement with that of Pantelides *et al.*)

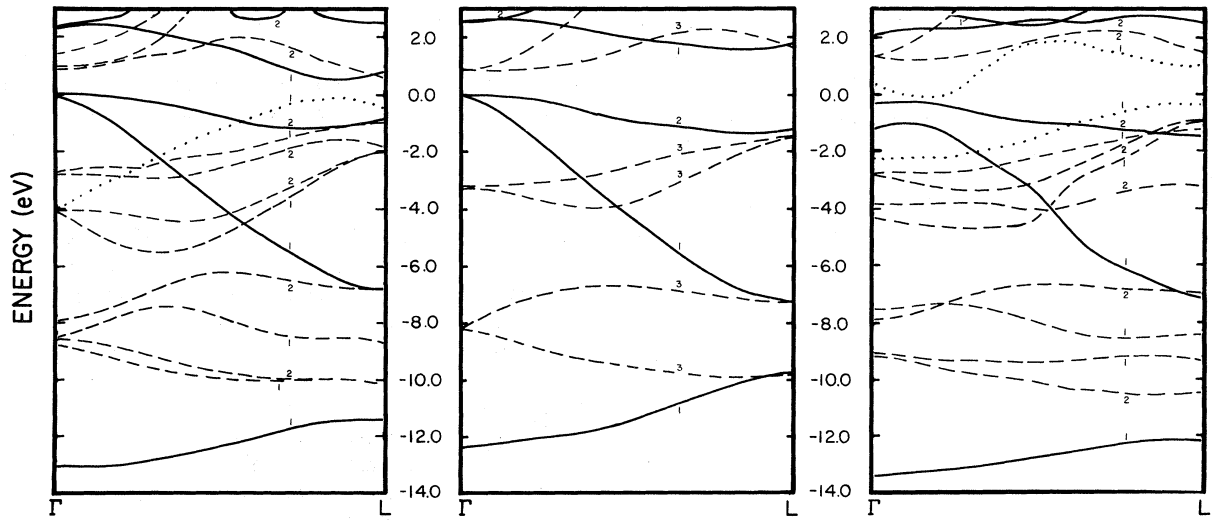

FIG. 3. Band structures for geometry I (unrelaxed). Center panel is for pure silicon. Left- and right-hand panels are for tetrahedral- and hexagonal-site interstitials, respectively.

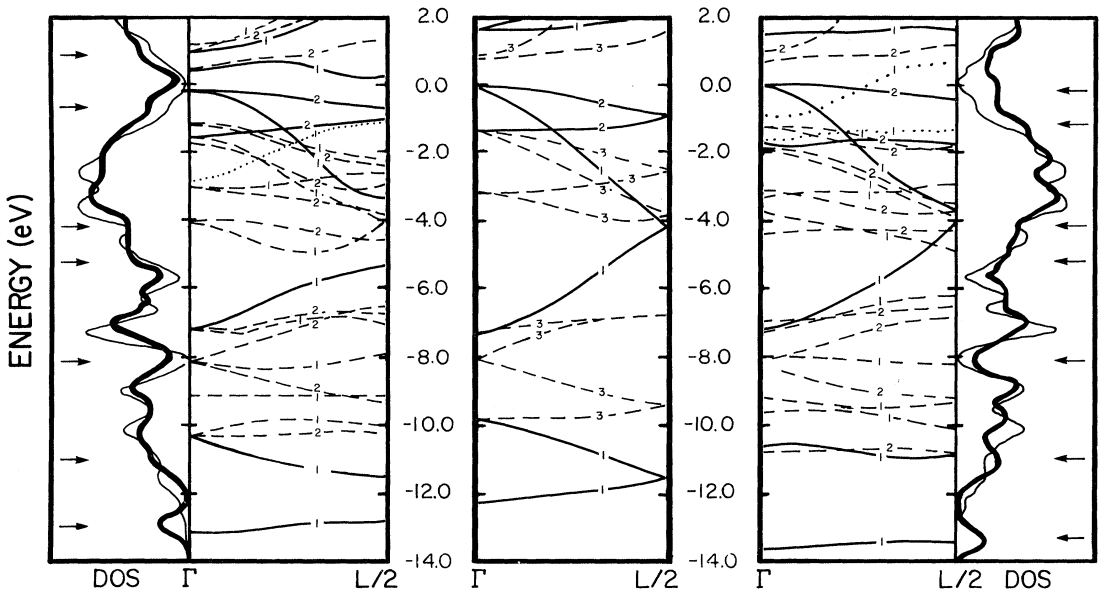

FIG. 4. Band structures for geometry II (unrelaxed) with density of states. Center panel is for pure silicon. Left- and right-hand panels are for tetrahedral- and hexagonal-site interstitials, respectively. Thick solid line in DOS plots are for geometries with the interstitial; thin solid line is the pure-silicon DOS for comparison.

1. Tetrahedral site

Looking first at the tetrahedral site we have placed arrows pointing to defectlike states and resonances on the density-of-states curves. We recognize these states as being "defectlike" by changes in the density of states and by looking at charge-density plots which display the nature of the states. Contour plots of the charge density of these states are given in Figs. 5(a)—(g) in order of decreasing binding energy.

From charge densities we can identify the characteristics of these states (some symmetry information is obtained by looking at the degeneracies and the wave function itself). To clarify the charge-density contour plots we describe the neighboring atoms of the tetrahedral interstitial [compare Fig. 1(a)]. There are four nearest neighbors of the interstitial which are located in a tetrahedral configuration at a distance equal to the bulk silicon-silicon distance. Two of these atoms are located in the plane of the charge-density plots; they are the atoms of the connected chain displaced upwards. There are six second-nearest neighbors located on the faces of the conventional unit cell at a distance 15% larger than the bulk silicon-silicon distance. Two of these atoms are shown in the plane of the charge-density plots located directly above and below the interstitial. The final set of atoms which are important in the description of electronic states is actually comprised of fourth-nearest neighbors which are at a distance of twice the bulk silicon-silicon distance. Of the eight fourth-nearest neighbors which are located at the corners of the conventional cube only four are important. These four are the outer ends of straight lines of three atoms which start on the interstitial and pass through the first-nearest neighbors. Two of these atoms are in the plane of the charge-density plots. For convenience of reference they will be called corner atoms. As will become clear, the three-atom linear chains are an important

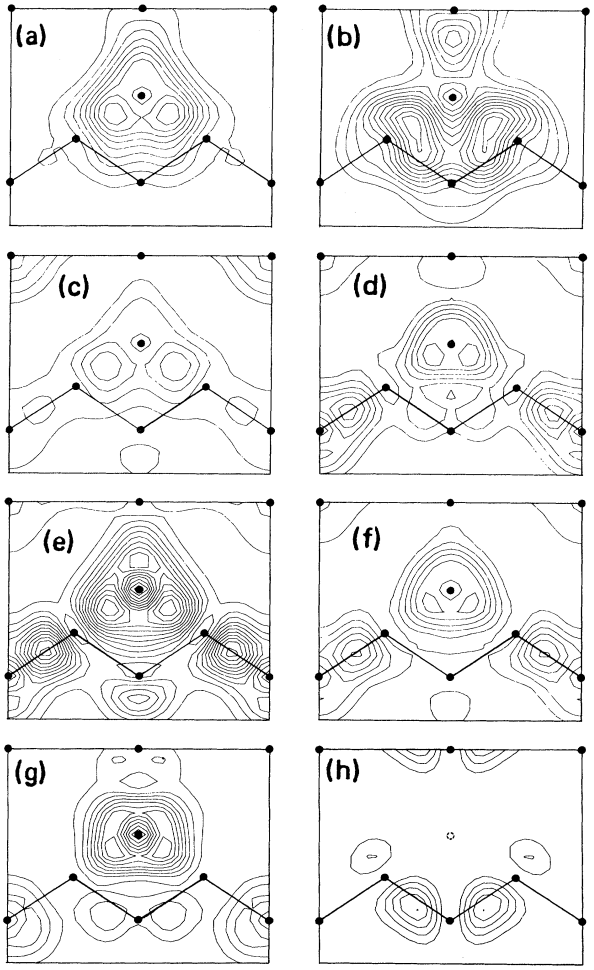

FIG. 5. Charge densities of tetrahedral-site interstitial associated electronic states. See text for details.

factor in the electronic states of the interstitial.

The defect-associated states in Figs. 5(a)—5(g) can be described as follows.[21]

(a) At -13 eV, a state of A_1 symmetry (thus s-like on the interstitial) has dropped out of the bottom of the valence band and can be seen to be almost exclusively s-like on the interstitial with some bonding to nearest neighbors.

(b) At -11 eV, a resonance of T_2 symmetry (thus p-like on the interstitial) shows strong bonding of p-like interstitial orbitals with s orbitals on first- and second-nearest neighbors.

(c) At -8 eV, there is a resonance of primarily A_1 character. The charge density shown shows that this state is surprisingly extended and is thus characteristic of the host. Thus, the supercell used may not be sufficiently large to give an accurate charge density.

At -5.5 and -7 eV two peaks appear in the density of states, which, upon looking at the charge density, are actually bulk-like states. Closer inspection shows that the peaks are most likely a result of inaccuracy in our density of states and would be eliminated with a better sampling of the Brillouin zone.

(d) At -5 eV, there is a resonance of A_1 symmetry with strong bonding to p-like orbitals on the first-nearest neighbors and both s- and p-like states on the corner atoms.

(e) At -4 eV, a resonance of T_2 symmetry which is a clear companion to the A_1 state at -5 eV shows bonding to p-like states on the corner atoms and some p-like character on the second-nearest neighbors.

(f) At -0.5 eV, the final resonance in the valence band with interstitial character is the state which was pulled down from the conduction band. Having A_1 symmetry it can be seen to be s-like on the interstitial bonding to p-like states on the corner atoms.

(g) The companion of the A_1-like state at -0.5 eV is in the conduction band at $+1.5$ eV.

We observe that these results show that there is a relatively small A_1-T_2 splitting of about 2 eV which results in the pairing of states as follows: (a) and (b), (d) and (e), and (f) and (g).

Finally, we note that special care must be taken in the interpretation of charge densities to identify defect states. For example, in Fig. 5(h) we show a state of T_1 symmetry which appears to be associated with the defect. However, this state was obtained by breaking the crystal Hamiltonian symmetry to tetrahedral-site symmetry without the presence of an interstitial. We distinguish defect states from bulklike states by comparing such symmetry-broken bulk states with states of the interstitial calculation.

2. *Hexagonal site*

Moving to the hexagonal site, the states are complicated by symmetry breaking leading to degeneracy splitting. The $[\bar{1}11]$ direction is no longer equivalent to the [111] direction. For our purposes we will continue to consider only the [111] direction as shown in Figs. 3 and 4.

The most important structural feature which determines the nature of electronic states is the buckled hexagonal ring formed of nearest neighbors which is perpendicular to the plane of the charge-density plots. These nearest neighbors are at a distance of 96% of the bulk silicon-silicon distance. Two of them are in the plane of the charge-density plots and can be easily identified as the atoms closest to the interstitial. Charge-density plots for the hexagonal site are given in Fig. 6.

Most of the defect-associated states identified at the tetrahedral site can be followed over to the hexagonal site. Energies and characteristics change somewhat during the movement. A_1 states become A_1^+ and T_2 states split into one A_2^- and two E^- states With one important exception the A_2^- state becomes bulklike.

(a) The defect state which dropped out of the bottom of the valence band drops still further and is now located at -13.5 eV. It has A_1^+ symmetry and can be seen to be largely s-like, but flattened and stretched in the hexagonal ring.

(b) The companion T_2 state is now of E^- symmetry and forms a torus of charge in the hexagonal ring. Its energy is only slightly lowered.

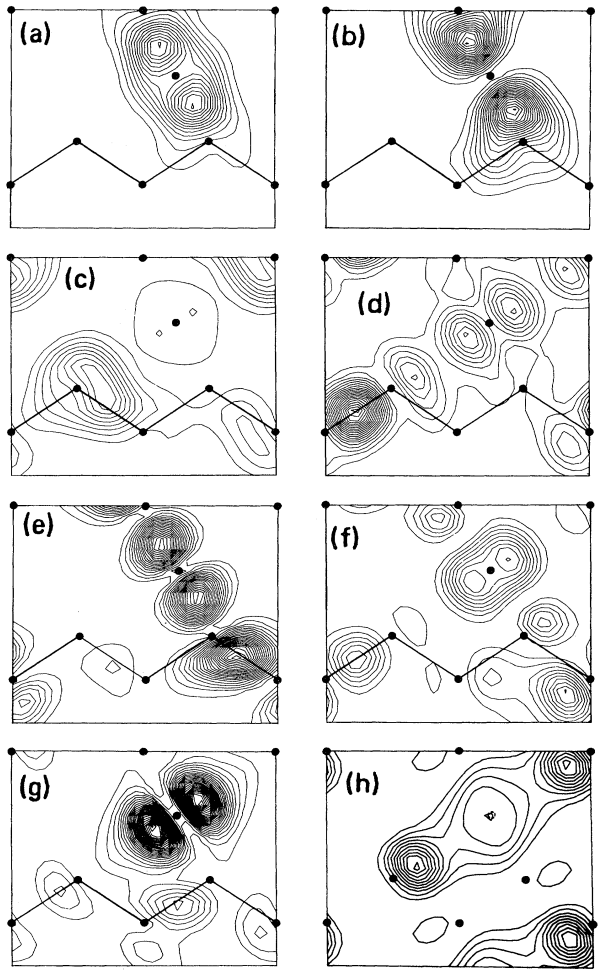

FIG. 6. Charge densities of hexagonal-site interstitial associated electronic states. See text for details.

(c) The state in the s-p gap (A_1^+) remains surprisingly extended and seems to have transformed to a nonbonding s orbital on the diagonally displaced atoms. It is difficult to identify as a defectlike state.

(d) and (e) The next pair of states at -5 and -4 eV (A_1^+ and E^-) can again be seen to be comprised of bonding states with further neighbors. [For comparison of the density of states (DOS) with the band structure we note that the state at -5 eV has higher energy along the [111] direction in this geometry.]

(f) and (g) Finally, the two states which have dropped from the conduction band are s-like and p-like at -0.5 and 0 eV, respectively. The state at the bottom of the gap is remarkable in that it is almost pure p perpendicular to the plane of the hexagonal ring. Thus it is almost completely nonbonding to the crystal. This is the unique A_2^- state associated with the defect. Here, again, in Fig. 6(h) we show a bulk state which can be obtained by symmetry-breaking the crystal Hamiltonian.

C. Relaxation

We now investigate the effects of relaxation. The total-energy breathing-mode–relaxation calculation of nearest neighbors which will be described in Sec. IV leads to the result that the nearest neighbors relax outwards by 3.5% at the tetrahedral site and 5% at the hexagonal site. Total valence charge densities for this case were shown in Fig. 2 with the relaxed and unrelaxed positions indicated for comparison. The band structures are given in Fig. 7.

Generally, the effect of relaxation on the defect electronic states is either to cause them to become more extended or less extended depending on the nature of their bonding to the crystal. For example, the lowest-lying level which is bonding in nature becomes more extended upon outward relaxation and moves upward in energy, whereas the defect state at -5 eV—which is nonbonding—tends to become slightly more localized.

D. Charge-density changes

In Fig. 8 we show the charge-density difference upon adding the $Si^{(2+)}$ interstitial at the tetrahedral and hexagonal sites. We see the rapid decay of the electron charge density contributed by adding an interstitial atom.

In Fig. 9 we show the change in charge density upon relaxation. Relaxation expands the region of influence of the interstitial. In particular, the relaxation increases the nearest-neighbor bond distance and transfers charge from the interstitial "overbonded" nearest-neighbor bonds to the contracting bonds further away (reflecting the deepening of those bond potentials).

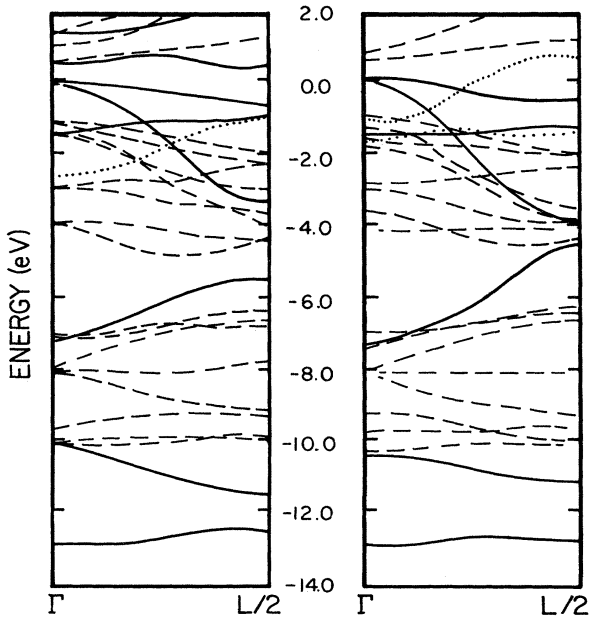

FIG. 7. Band structures for geometry II (relaxed). Left- and right-hand panels are for tetrahedral- and hexagonal-site interstitials, respectively.

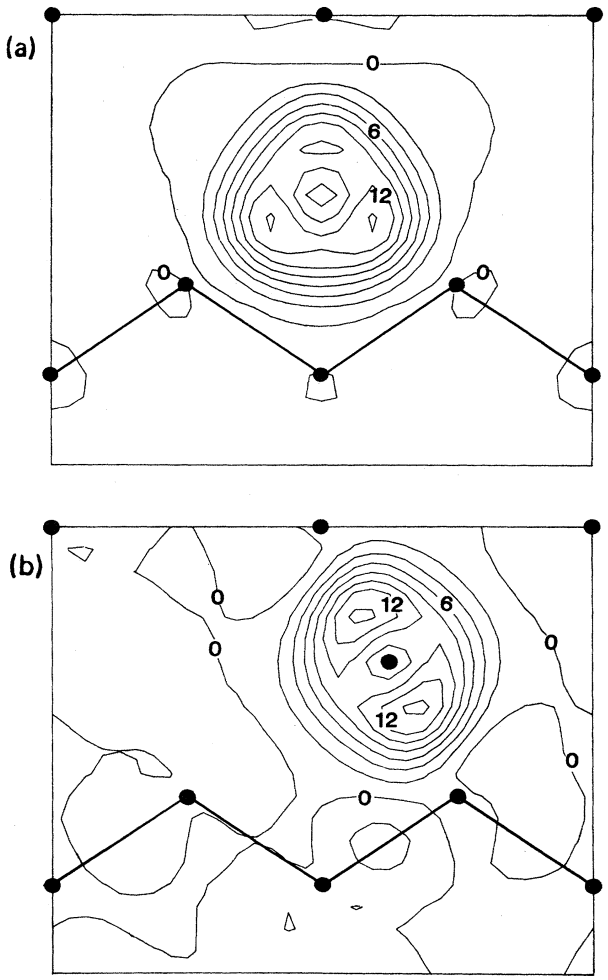

FIG. 8. Total valence charge-density differences upon adding an interstitial (in units of electrons per bulk primitive cell) (a) at a tetrahedral site and (b) at a hexagonal site.

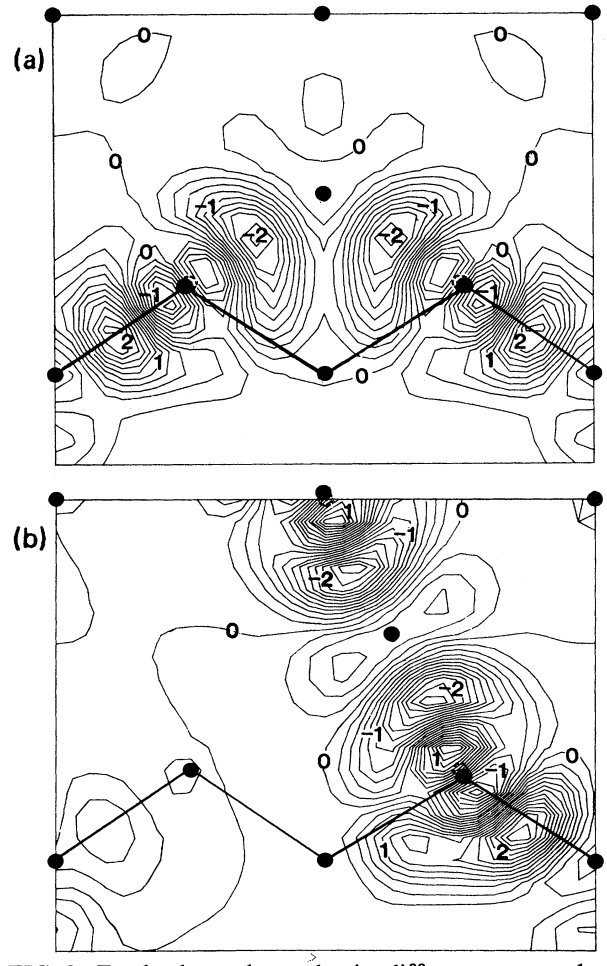

FIG. 9. Total valence charge-density differences upon relaxation (in units of electrons per bulk primitive cell) (a) at a tetrahedral site and (b) at a hexagonal site.

TABLE I. Migration energy barriers (in eV).

	Unrelaxed	Relaxed
$Si^{(2+)}$	1.9±0.1	1.2±0.2
$Si^{(0)}$	0.5±0.3	1.2±0.3

IV. TOTAL-ENERGY MIGRATION-BARRIER CALCULATIONS

We now proceed to a description of the total-energy results and describe migration-barrier and relaxation calculations. The results for $Si^{(0)}$ and $Si^{(2+)}$ migration barriers in *p*-type silicon are presented in the left-hand panel of Fig. 10 and in Table I.

As before, we first consider the case of placing the interstitial in an ideal host environment without allowing the crystal atoms to distort. The total-energy migration curves are shown as dashed lines in Fig. 2. We observe that the energy curve for $Si^{(0)}$ is relatively flat with a (0.5±0.3)-eV barrier to migration. The stable-charge state, however, is $Si^{(2+)}$ which has a large migration barrier of (1.9±0.1) eV and a minimum-energy position at the tetrahedral site.

We now allow the host-crystal atoms to relax. Since the filled electronic states for both $Si^{(0)}$ and $Si^{(2+)}$ are nondegenerate, symmetry-breaking (Jahn-Teller) distortions of the lattice sites should not be important. Thus we consider nearest-neighbor breathing-mode relaxation at the tetrahedral site as a first approximation to the relaxation. Relaxation was studied by evaluating the total energy at 0%, 5%, and 10% relaxation of nearest-neighbor bond distances. A parabola was fitted to these points to determine the minimum energy and relaxation distance. For the hexagonal site, total energy was minimized in a

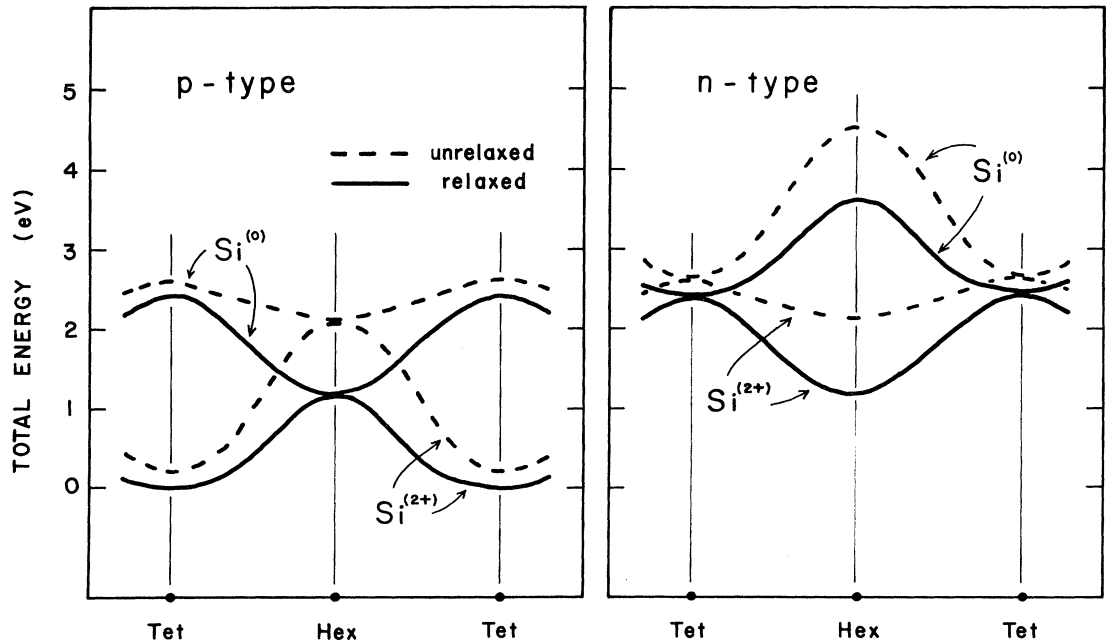

FIG. 10. Silicon self-interstitial migration barriers for unrelaxed and relaxed $Si^{(0)}$ and $Si^{(2+)}$ along the [111] direction for *p*-type (left-hand panel) and *n*-type (right-hand panel) silicon. The zero of energy is arbitrarily set at the *p*-type minimum-energy site.

TABLE II. Relaxation of nearest neighbors in units of bulk silicon-silicon nearest-neighbor distance and associated energy change. For the hexagonal site, (a) represents breathing, and (b) represents ring buckling (see text).

	Tetrahedral		Hexagonal	
	Relaxation (%)	Energy change (eV)	Relaxation (%)	Energy change (eV)
$Si^{(2+)}$	3.0±1.0	−0.24±0.1	(a) 4.1±1.0	−0.74±0.2
			(b) 2.3±1.0	−0.16±0.1
$Si^{(0)}$	3.2±1.0	−0.26±0.1	(a) 4.2±1.0	−0.80±0.2
			(b) 2.3±1.0	−0.10±0.1

two-parameter space including breathing and buckling (displacing three atoms of the ring in the [111] direction and three in the opposite direction, thus preserving symmetry). Results are presented in Table II. We note that the relaxation energies of $Si^{(0)}$ and $Si^{(2+)}$ are essentially the same.

The most dramatic result from the relaxation studies is that the hexagonal-site relaxation energy is much greater than the tetrahedral-site relaxation energy, the difference being ~0.7 eV. Thus the barriers are significantly changed by the relaxation. The $Si^{(0)}$ migration barrier is found to be (1.2±0.3) eV and is stable at the hexagonal site. The $Si^{(2+)}$ migration barrier is reduced to (1.2±0.2) eV and remains stable at the tetrahedral site.

In the right-hand panel of Fig. 10 we display the results for *n*-type silicon. These are obtained simply by shifting the $Si^{(2+)}$ curves with respect to the $Si^{(0)}$ curves by twice the gap energy, which corresponds to moving the Fermi level from the top of the valence band to the bottom of the conduction band. Thus we see that in *n*-type silicon the stable charge state is $Si^{(0)}$, and that it is stable at the hexagonal site.

V. CONCLUDING REMARKS

Our calculations show that electron-assisted migration occurs. The electron-assisted transport mechanism is the Bourgoin mechanism[7] which proceeds as follows. In *p*-type silicon the stable silicon interstitial will be $Si^{(2+)}$ at the tetrahedral site (see Fig. 10). In the presence of electrons excited into the conduction band by irradiation, $Si^{(2+)}$ can capture two electrons and become $Si^{(0)}$. Since it is unstable it will fall to the hexagonal site. Then it can capture two holes, become $Si^{(2+)}$, and then fall to the tetrahedral site, providing a mechanism for transport even if thermal energy will not enable crossing of the barrier.

In *n*-type silicon electron-assisted migration will also occur, as can be seen from the right-hand panel of Fig. 10. Proceeding now, $Si^{(0)} \rightarrow Si^{(2+)} \rightarrow Si^{(0)}$.

Since electron-assisted transport occurs for the two-electron process,

$$Si^{(2+)} \rightarrow Si^{(0)} \rightarrow Si^{(2+)} ,$$

it is clear that electron-assisted transport must occur for a single-electron process,

$$Si^{(2+)} \rightarrow Si^{(+)} \rightarrow Si^{(2+)}$$

or

$$Si^{(0)} \rightarrow Si^{(+)} \rightarrow Si^{(0)} .$$

These one-electron processes will also occur in irradiated systems. The $Si^{(+)}$ barrier can be obtained to reasonable accuracy by averaging the $Si^{(2+)}$ and $Si^{(0)}$ barriers. Our study indicates that the $Si^{(+)}$ barrier may in fact be very low and thus may enable electron-assisted transport for both single-electron mechanisms.

Finally, we would like to note that after this manuscript was written we became aware of recent similar total-energy calculations[22,23] using a Green's-function approach, the results of which are generally consistent with ours.

Note added in proof. It has come to our attention that *semiempirical* total-energy calculations of high-symmetry interstitial configurations have been attempted by P. Masri *et al.*[24] Our conclusions differ from those of P. Masri *et al.*; however, direct comparison is difficult because of large error bars dictated by self-consistency tests of their results.

ACKNOWLEDGMENTS

We would like to thank Dr. S. T. Pantelides and Dr. G. D. Watkins for introducing us to this problem. This work was supported in part by U. S. Office of Naval Research Grant No. N00014-77-C-0132. One of us (Y.B.) would like to acknowledge support by the National Science Foundation.

APPENDIX: $Si^{(0)}$ ENERGY-EIGENVALUE CORRECTION

In order to obtain accurate total-energy calculations for $Si^{(0)}$ it was necessary to make a correction to the contribution of the highest occupied energy level (unoccupied for $Si^{(2+)}$).

At the tetrahedral site this energy level can be seen from Fig. 4 to be in the conduction band. If we take the large supercell limit of this calculation we see that the contribution of this eigenvalue will be that of a hydrogenic level just below the bottom of the conduction band. The current calculations using density-functional theory places this level at an energy of 0.6 eV above the valence band (i.e., the gap is 0.6 eV instead of 1.2 eV). Thus we must make a correction to the eigenvalue to place it at the correct energy above the valence-band maximum.

At the hexagonal site there is no need to correct the eigenvalue for the band-gap error since now it is at the top of the valence band [see Figs. 4 and 6(g)].

[1]See, e.g., M. T. Yin and Marvin L. Cohen, Phys. Rev. Lett. **45**, 1004 (1980); Phys. Rev. B **26**, 5668 (1982); and other articles cited in Refs. 2–4.

[2]M. T. Yin and Marvin L. Cohen, Phys. Rev. B **24**, 2303 (1981); John E. Northrup and Marvin L. Cohen, Phys. Rev. Lett. **49**, 1349 (1982).

[3]J. Ihm and J. D. Joannopoulos, Phys. Rev. Lett. **47**, 679 (1981); **47**, 1568(E) (1981); Phys. Rev. B **26**, 4429 (1982).

[4]David Vanderbilt and J. D. Joannopoulos, Solid State Commun. **35**, 535 (1980); Phys. Rev. Lett. **49**, 823 (1982); G. A. Baraff and M. Schlüter, Phys. Rev. B **28**, 2296 (1983).

[5]Y. Bar-Yam and J. D. Joannopoulos, Phys. Rev. Lett. **52**, 1129 (1984).

[6]G. D. Watkins, J. R. Troxell, and A. P. Chatterjee, in *Proceedings of the International Conference on Radiation Effects in Semiconductors, Nice, 1978,* edited by J. H. Albany (IOP, London, 1979), p. 16; G. D. Watkins, in *Proceedings of the International Conference on Defects in Semiconductors, Freiburg, West Germany, 1974* (IOP, London, 1975), p. 1.

[7]For a review of high-temperature diffusion measurements, see Werner Frank, Ulrich Gosele, Helmut Mehrer, and Alfred Seeger, in *Diffusion in Solids II,* edited by A. S. Nowick and G. Murch (Academic, New York, in press).

[8]J. C. Bourgoin and J. W. Corbett, in *Proceedings of the International Conference on Defects in Semiconductors, Freiburg, West Germany, 1974,* Ref. 7, p. 149; Phys. Lett. **38**, 135 (1972).

[9]See *Defects in Semiconductors,* Vol. II of *Materials Research Society Symposium Proceedings,* edited by J. Narayan and T. Y. Tan (North-Holland, Amsterdam, 1981).

[10]G. D. Watkins, R. P. Messmer, C. Weizel, D. Peck, and J. W. Corbett, Phys. Rev. Lett. **27**, 1573 (1971).

[11]S. T. Pantelides, I. Ivanov, M. Scheffler, and J. P. Vigneron, Physica **116B**, 18 (1983).

[12]J. K. Nørskov and N. D. Lang, Phys. Rev. B **21**, 2131 (1980); M. J. Stott and E. Zaremba, Solid State Commun. **32**, 1297 (1979).

[13]G. A. Baraff, M. Schlüter, and G. Allan, Phys. Rev. Lett. **50**, 739 (1983).

[14]Y. Bar-Yam and J. D. Joannopoulos, Phys. Rev. B **30**, 2216 (1984).

[15]D. Hamann, M. Schlüter, and C. Chiang, Phys. Rev. Lett. **43**, 1494 (1979).

[16]G. B. Bachelet, D. Hamann, and M. Schlüter, Phys. Rev. B **26**, 4199 (1982).

[17]J. Perdew and A. Zunger, Phys. Rev. B **23**, 5048 (1981); D. M. Ceperley and B. J. Alder, Phys. Rev. Lett. **45**, 566 (1980).

[18]Cosmetic differences between the total-energy results reported here and those reported earlier (Ref. 5) are due to the addition of the *d* nonlocal component to the pseudopotential.

[19]J. Ihm, Alex Zunger, and Marvin L. Cohen, J. Phys. C **12**, 4409 (1979).

[20]D. J. Chadi and Marvin L. Cohen, Phys. Rev. B **12**, 5747 (1973).

[21]Symmetry notation is as in M. Tinkham, *Group Theory and Quantum Mechanics* (McGraw-Hill, New York, 1964), Appendix B. We use (+) to indicate the character under inversion.

[22]G. A. Baraff and M. Schlüter (unpublished).

[23]Roberto Car, Paul J. Kelly, Atsushi Oshiyama, and Sokrates T. Pantelides, Phys. Rev. Lett. **52**, 1814 (1984).

[24]P. Masri, A. H. Harker, and A. M. Stoneham, J. Phys. C **16**, L613 (1983).